RSC Advances

PAPER

View Article Online
View Journal | View Issue



Cite this: *RSC Adv.*, 2015, **5**, 102392

# Insight into ETS-10 synthesis for the preparation of mixed matrix membranes for $CO_2/CH_4$ gas separation†

Sara Sorribas,[a] Bibiana Comesaña-Gándara,[b] Angel E. Lozano,[bc] Beatriz Zornoza,[a] Carlos Téllez[a] and Joaquín Coronas*[a]

Received 29th September 2015
Accepted 19th November 2015

DOI: 10.1039/c5ra20172a

www.rsc.org/advances

An in-depth study into the synthesis of the titanosilicate ETS-10 has been carried out to obtain crystals with different particle sizes, roughness and porosity. The effect of these parameters on the $CO_2/CH_4$ gas separation performance using mixed matrix membranes (MMMs) has been studied. MMMs based on ETS-10 polycrystalline particles of 1–2 μm in size with high surface roughness and porosity gave rise to a good filler dispersion and filler–polymer interaction. The addition of 10 wt% ETS-10 polycrystalline particles into the polysulfone matrix increased the $CO_2$ permeability from 6.1 to 7.8 Barrer and the $CO_2/CH_4$ selectivity from 31 to 38. When using the polyimide 6FDA-6FpDA, a glassy polymer with high gas permeability, the addition of 10 wt% ETS-10 polycrystalline particles increased the $CO_2$ permeability from 96 to 125 Barrer, with a decrease in $CO_2/CH_4$ selectivity from 56 to 51.

## 1. Introduction

ETS-10 is a microporous titanosilicate with the formula $M_2TiSi_5O_{13}\cdot nH_2O$ (where M = K, Na), built from orthogonal $TiO_6$ octahedra and $SiO_4$ tetrahedra linked by corner-sharing oxygen atoms forming a three-dimensional pore system with good accessibility for guest molecules.[1] Each Ti atom in a six-coordinated state carries two negative charges balanced by $Na^+$ and $K^+$ cations, which give this material a high cation exchange capacity.[2] The synthesis of the titanosilicate ETS-10 was first reported by Kuznicki, who used $TiCl_3$ as the Ti source along with seeds of ETS-4.[3] Since then, substantial efforts have been made to grow highly crystalline pure ETS-10 in conventional hydrothermal syntheses (at temperatures between 150–230 °C) and short time periods (<48 h).[4] In addition, several studies have focused on controlling nucleation/crystal growth processes as a way to modify the ETS-10 particle size, a critical parameter when synthesizing zeolitic materials for a specific application.[5] For example, while large sizes allow structure refinement from single crystal data and studying the formation of intergrowth structures inside single zeolite crystals,[6,7] small sizes[8–10] may have applications in the preparation of mixed matrix membranes (MMMs) for molecular separations.

MMMs are an excellent strategy to overcome the trade-off between permeability and selectivity for polymeric membranes. The use of two materials with different gas separation behaviors offers the possibility of designing an efficient membrane combining the advantages of both phases: the easy processability and low cost of the polymer with the superior gas separation performance of the nanostructured fillers.[11–13] Also, the incorporation of these specific materials within the polymeric matrix generally provides enhanced physical, mechanical and thermal properties for their use in aggressive environments and a membrane stabilization system against changes in permeability with the temperature.[14]

ETS-10 inorganic membranes on α-alumina supports have previously been used in the separation of propylene/propane mixtures,[15,16] and in the separation of $CO_2$ mixtures ($CO_2/N_2$, $CO_2/H_2$),[17] since ETS-10 is a basic nature material which can adsorb $CO_2$ at low temperatures.[18] Regarding MMMs based on the titanosilicate ETS-10, Burmann *et al.*[19] prepared 8 wt% ETS-10-polysulfone MMMs *via* spin coating for $H_2/CH_4$ and $O_2/N_2$ gas separation mixtures, obtaining a slight improvement in gas permeability/selectivity compared to the bare polymer film. Chitosan (CS) and microporous titanosilicate ETS-10/CS MMMs were prepared and tested for pervaporation of water/ethanol mixture increasing flux with respect to the pure CS membranes.[20]

Polysulfone (PSF), whose structure is shown in Fig. 1a, is an important commercial membrane material for gas separation due to its excellent mechanical properties, wide operating temperature range, fairly good chemical resistance, easy fabrication and low price.[21] However, its great rigidity due to its high

[a]*Chemical and Environmental Engineering Department and Instituto de Nanociencia de Aragón (INA), Universidad de Zaragoza, 50018 Zaragoza, Spain. E-mail: coronas@unizar.es; Fax: +34 976 761879; Tel: +34 976 762471*

[b]*Department of Macromolecular Chemistry, Institute of Polymer Science and Technology, ICTP-CSIC, 28006 Madrid, Spain*

[c]*SMAP, UVA-CSIC Research Unit, University of Valladolid, 47011 Valladolid, Spain*

† Electronic supplementary information (ESI) available. See DOI: 10.1039/c5ra20172a

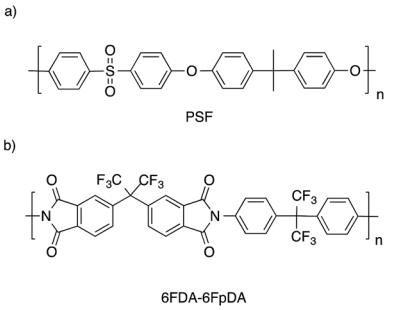


Fig. 1 Molecular structure of (a) PSF, (b) polyimide 6FDA-6FpDA.

degree of molecular immobility leads to low permeabilities. To improve the permeability and selectivity of gas separation polymeric membranes, the incorporation of bulky groups in the chains of glassy polymers makes their structure stiffer and hinders an efficient packing of the chains, leading to an increase in free volume. The high volume fractions with restrictive or selective channels increase the diffusivity of gases, and thus their permeability. An example of such a kind of polymer is the fluorinated polyimide 6FDA-6FpDA, whose structure is shown in Fig. 1b. Fluorinated polyimides are particularly interesting for gas separation because they have good mechanical, thermal and transport properties.[22] 6FDA-6FpDA is an aromatic polyimide having two hexafluoropropane moieties. This polyimide is soluble in many common organic solvents including acetone, tetrahydrofuran and chloroform, it has very good thermal stability and shows very good gas separation properties, in particular for mixtures where one of the components is $CO_2$.[22–25]

Here, the preparation of ETS-10 MMMs based on PSF *via* casting/solvent evaporation technique (in contrast with our previously reported ETS-10/PSF MMMs prepared by spin coating)[19] is studied. In addition, a more permeable fluorinated polymer, the polyimide 6FDA-6FpDA, is used as polymer matrix for the preparation of ETS-10 MMMs. In order to analyze the effect of the crystal size and morphology of the filler on the membrane performance, several ETS-10 crystals with different size and textural properties are synthesized and the MMMs are evaluated for separation of $CO_2/CH_4$ mixture. This mixture can be related to bio-methane upgrading, an application of special interest given the renewable character of such source of energy, whose use would contribute to reduce $CO_2$ emissions.

# 2. Experimental

## 2.1. Synthesis of ETS-10 crystals

Several syntheses were carried out by varying different parameters (Ti source, temperature and synthesis time). Table S1† summarizes all the syntheses conditions implemented. The nomenclature used here is "Ti source_ temperature_time". The different procedures followed to synthesize ETS-10 crystals are described below.

**2.1.1. Synthesis of ETS-10 crystals using $TiO_2$.** The preparation of ETS-10 crystals using $TiO_2$-anatase of two different sizes as the Ti source (Ti1 of 200–300 nm and Ti2 of 25 nm, both from Sigma-Aldrich, 99.8 and 99.7 wt%, respectively) was carried out as follows.[5] Firstly, 12.3 g of sodium silicate solution (27 wt% $SiO_2$, 8 wt% $Na_2O$, Merck) and 16.5 g of distilled water were mixed. Next, 0.86 g of potassium chloride (99.995 wt%, Panreac), 1.1 g of potassium fluoride (99 wt%, Aldrich) and 3.5 g of sodium chloride (pro-analyse, Merck) were added to the mixture under strong stirring. Finally, 0.8 g of $TiO_2$-anatase was added and stirred for another 30 min to obtain the gel. The pH was measured in a 1/100 diluted portion of the gel, making sure that it was always in the 10.4–10.6 range to avoid impurities.[26] The resulting gel was poured into a Teflon-lined autoclave and submitted to hydrothermal synthesis at the desired temperature and time. After that, the autoclave was removed from the oven and quenched under cold tap water to room temperature. The product was centrifuged several times with water and dried at 100 °C overnight.

**2.1.2. Synthesis of ETS-10 crystals using $TiCl_3$.** For the preparation of ETS-10 crystals with $TiCl_3$ as the Ti source, the following hydrothermal synthesis procedure was used.[5] Firstly, 5.1 g of $TiCl_3$ (15 wt% $TiCl_3$ in 10 wt% HCl, Merck) was mixed with 21.4 g of distilled water. To convert $TiCl_3$ to $TiCl_4$, 0.66 g of hydrogen peroxide (30 wt%, Sigma-Aldrich) was added. After that, 0.86 g of potassium chloride (99.995 wt%, Panreac), 1.0 g of sodium hydroxide (extra pure, Scharlau) and 6.1 g of sodium silicate solution were added under strong stirring. For seeding, previously prepared 500 nm ETS-10 crystals (synthesis Ti2_180_48 h) in 0.3 wt% with respect to the total weight of the gel were added at the end. After complete mixing of the precursors for 30 min, the procedure was the same as for syntheses with $TiO_2$. It is worth mentioning that for the syntheses with $TiCl_3$ carried out at 180 °C or at two stages (180–230 °C), the molar gel composition used was diluted twice.

## 2.2. Synthesis of polyimide 6FDA-6FpDA

The synthesis of high molecular weight 6FDA-6FpDA was carried out by reacting the dianhydride 6FDA and the aromatic diamine, 6FpDA, through an *in situ* silylation base-assisted process.[27,28] Both monomers were purified by sublimation under high vacuum (220 °C for 6FDA and 190 °C for 6FpDA).

A three-neck flask was equipped with a mechanical stirrer and a nitrogen inlet and outlet. The flask was filled with 20 mmol of 6FpDA diamine and 20 mL of *N*,*N*-dimehtylacetamide (DMAc), which was employed as the solvent. The mixture was stirred at room temperature until all the solid had dissolved. Then, the solution was cooled to 0 °C and the required amount of trimethylchlorosilane (TMSCl) (1 mol per mol amino group, 40 mmol) was slowly added, followed by the addition of pyridine (1 mol per mol amino group, 40 mmol). The solution was heated to room temperature and stirred for 15 min to ensure the formation of the silylated diamine in the appropriate cases. After this time, the solution was once more cooled to 0 °C, and 20 mmol of 6FDA was rapidly added along with 15 mL of DMAc. Finally, a small amount of 4-dimethylamine pyridine (DMAP) (0.1 mol per mol amino group, 4 mmol) was added followed by 5.0 mL of solvent. The reaction mixture was then stirred for 15

min at 0 °C after which the temperature was raised to room temperature and left overnight.

Cyclodehydration of the formed polyamic acid was accomplished by using an acetic anhydride (60 mmol)/Py (60 mmol) mixture. The reaction mixture was stirred at room temperature for 6 h followed by heating for a further hour at 60 °C. Afterwards, the flask was cooled down to room temperature and the resulting polymer solution was precipitated into 1000 mL of water, washed several times with water and extracted in a Sohxlet extractor with ethanol to remove traces of solvent and oligomers. The 6FDA-6FpDA polymer was dried overnight under vacuum at 200 °C in order to remove the occluded solvent. Yield over 91% was obtained.

### 2.3. Preparation of MMMs

Two different polymers were used as matrices to prepare MMMs, commercial PSF (Aldrich, $M_w$ 35 000) and polyimide 6FDA-6FpDA. ETS-10 MMMs were prepared by the casting/solvent evaporation technique using chloroform as solvent. Firstly, 3.6 g and 4.2 g of chloroform (Sigma Aldrich, 99%) for PSF and 6FDA-6FpDA based MMMs, respectively, together with the amount of ETS-10 necessary to obtain the required loading (10–20 wt%) were mixed, keeping the amount of ETS-10 + polymer = 0.4 g. The polymer (PSF or 6FDA-6FpDA) was then added and the resulting dispersion was stirred overnight. The suspension was then sonicated with three intervals of 15 min, cast on a flat glass plate and then left overnight, partially covered to slow down the natural evaporation of solvent under ambient conditions. Once dried at room temperature, the films were placed for 24 h under 1 kPa pressure in a vacuum oven at 120 °C for PSF based MMMs and at 180 °C for 6FDA-6FpDA based MMMs to remove the remaining solvent.

### 2.4. Characterization

To analyze the ETS-10 particle size and morphology, and to evaluate their dispersion and the contact between the ETS-10 and the polymeric phase, both ETS-10 powder and the MMMs were characterized by scanning electron microscopy (SEM) using an Inspect F scanning electron microscope. Prior to observation, the samples were coated with 15 nm of platinum. MMM cross sections were prepared by freeze-fracturing after immersion in liquid $N_2$ before coating.

The ETS-10 samples and MMMs based on 6FDA-6FpDA were also characterized by X-ray diffraction (XRD) at room temperature using a D-Max Rigaku diffractometer with a copper anode and a graphite monochromator to select Cu-$K_{\alpha 1}$ radiation ($\lambda$ = 1.5418 Å).

Nitrogen adsorption–desorption isotherms were measured at 77 K using a porosity analyzer (TriStar 3000, Micromeritics Instrument Corp.). The samples were outgassed with a heating rate of 10 °C $min^{-1}$ until 200 °C and maintained for 8 h. BET specific surface areas were measured from the adsorption branches in the relative pressure range of 0.05–0.25 and external surface areas were calculated using the *t*-plot method.

### 2.5. Permeation measurements

The gas permeation equipment used in the study is described elsewhere.[29] For permeation tests, 13.8 $cm^2$ circular membranes were cut from the films prepared as described above. The membrane samples were placed in a module consisting of two stainless steel pieces and a macroporous disk support 316LSS of 20 μm nominal pore size, gripped inside with Viton o-rings. An equimolar mixture of 25/25 $cm^3$ (STP) per min $CO_2/CH_4$ stream was fed at 330 kPa to the retentate side of the membrane using mass-flow controllers, while the permeate side of the membrane was swept with a 2 $cm^3$ (STP) per min mass-flow controlled stream of helium at 125 kPa. The differential pressure between the retentate and the permeate side ($\Delta P$) was 205 kPa. Concentrations of $CO_2$ and $CH_4$ in the outgoing streams were analyzed by an Agilent 3000A online gas microchromatograph equipped with a thermal conductivity detector. Permeability in Barrer ($1 \times 10^{-10}$ $cm^3$ (STP) cm per ($cm^2$ s cmHg)) was calculated once the exit stream of the membrane was stabilized, and the separation selectivity was calculated as the ratio of permeabilities. To calculate the ideal selectivity and compare the results with those given in the literature, single gas measurements were also carried out for 6FDA-6FpDA membranes by feeding 50 $cm^3$ (STP) per min of individual gases, $CO_2$ and $CH_4$, at 330 kPa. The temperature of the experiments was controlled at 35 °C.

## 3. Results and discussion

### 3.1. Characterization of ETS-10 crystals

To obtain ETS-10 crystals with different particle size and roughness, several syntheses were carried out by varying parameters such as the Ti source, temperature and synthesis time (see Table S1 in the ESI†). In brief, from a reference synthesis at 230 °C using $TiCl_3$,[5,30] the temperature was decreased down to 180 °C and/or $TiO_2$ anatase of two different sizes (25 and 200–300 nm) was used as a low solubility Ti source to slow the crystal growth and thus have an effect on the particle size. The aim of testing different ETS-10 crystals as fillers was to study the effect of the particle size on the separation performance of the MMMs and to improve the bonding established between the polymer and the filler by increasing the external roughness of the ETS-10 particles.[31]

Fig. 2 and 3 and Table 1 show SEM images, X-ray diffraction patterns and textural properties, respectively, of the different samples selected for the preparation of the MMMs. Table 1 also shows the ETS-10 particle size, in both *c* and $a = b$ directions.[32]

Sample Ti2_180_48 h (Fig. 2a) was synthesized with $TiO_2$-anatase nanoparticles (25 nm), which led to a heterogeneous primary nucleation of ETS-10.[5] This, together with its low solubility, dramatically reduced the availability of nutrients for growth, leading to small ETS-10 particles (0.44 × 0.21 μm). It is worth mentioning that at 180 °C it was not possible to obtain ETS-10 crystals with Ti1 (200–300 nm), since this Ti source needs higher temperatures to be dissolved. In general, when using the same synthesis conditions (*i.e.* 230 °C and 48 h), larger crystal particles were obtained with $TiCl_3$ (see Table S1 and

 

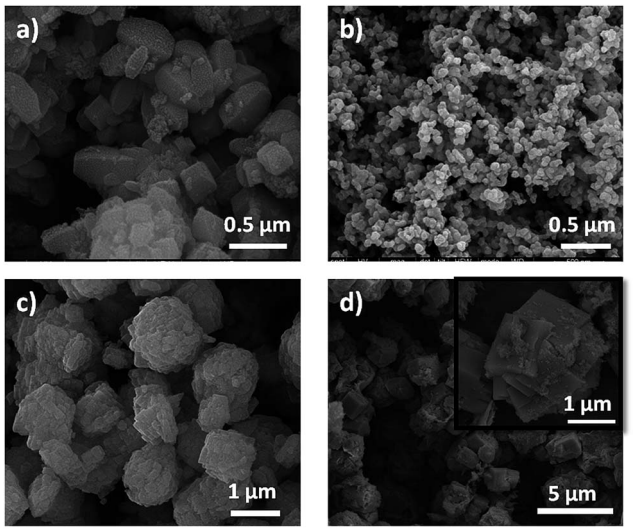


Fig. 2 SEM images of ETS-10 samples used for MMM preparation: (a) Ti2_180_48 h, (b) $TiCl_3$_180_48 h, (c) $TiCl_3$_180–230_48–2 h, (d) $TiCl_3$_180–230_48–24 h.

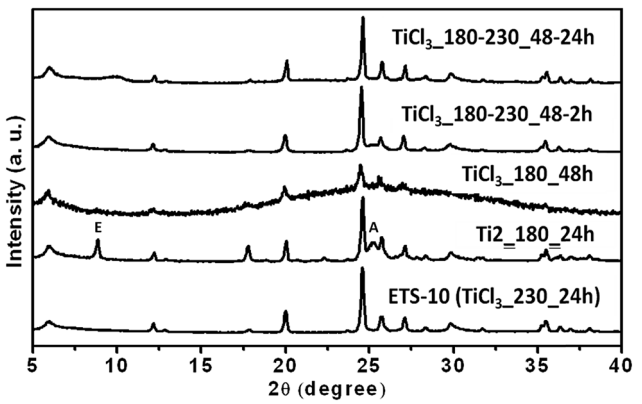


Fig. 3 XRD of ETS-10 samples used for MMM preparation: conventional ETS-10 synthesis ($TiCl_3$_230_24 h), Ti2_180_48 h, $TiCl_3$_180_48 h, $TiCl_3$_180–230_48–2 h and $TiCl_3$_180–230_48–24 h. E and A letters refer to ETS-4 and anatase impurities, respectively.

Fig. S1, ESI†), due to the promotion of crystal growth over nucleation when this more soluble Ti source was used.[5]

When the temperature was reduced to 180 °C and the molar gel was diluted (sample $TiCl_3$_180_48 h), nanocrystals of 80 ± 20 nm were obtained (Fig. 2b) with the presence of amorphous gel detected by XRD (see Fig. 3). This fact could be due to the low temperature used, which was insufficient to dissolve all the nutrients for crystal growth. It is worth mentioning that this is the smallest particle size ever reported for this material.[5,26,30,33] In sample Ti2_180_48 h, ETS-4 and $TiO_2$-anatase impurities were also present (see Fig. 3).

To increase the crystallinity of the $TiCl_3$_180_48 h sample, after 48 h at 180 °C the gel synthesis was heated up to 230 °C and maintained for 2 h (sample $TiCl_3$_180–230_48–2 h, Fig. 2c) and 24 h (sample $TiCl_3$_180–230_48–24 h, Fig. 2d). The increase in synthesis temperature to 230 °C increased the particle size to 1.2 ± 0.2 μm and 1.9 ± 0.3 μm after 2 h and 24 h, respectively. The crystallinity and porosity of these two samples were also higher than those for the $TiCl_3$_180_48 h sample (see Fig. 3 and Table 1), indicating that when $TiCl_3$ is used temperatures higher than 180 °C are needed to crystallize the titanium and silicon nutrients. SEM images of these samples (Fig. 2c and d) show particles consisting of polycrystalline aggregates that became twin crystals after 24 h, different from those of the $TiCl_3$_230_24 h sample (Fig. S1b, ESI†) which exhibits the typical truncated pyramidal crystal shape. The particles in Fig. 2c and d show an evident surface roughness that could be due to two reasons. Firstly, the dilution of the initial synthesis mixture resulting in crystal clusters, as previously reported.[4] Secondly, the presence of ETS-10 nanocrystals (Fig. 2b) generated at the 180 °C stage that act as seeds when the temperature is increased to 230 °C and grow close each other, creating polycrystalline particles.

The external surface of these samples was in accordance with their particle size and roughness. The $TiCl_3$_180_48 h sample had the highest external surface area (59 $m^2\ g^{-1}$) due to its having the smallest particle size (80 nm) in addition to the particle agglomeration that led to capillarity condensation between the crystals. Furthermore, samples $TiCl_3$_180–230_48–2 h and $TiCl_3$_180–230_48–24 h have extra roughness due to the intercrystalline regions, leading to high external specific surface areas (41–42 $m^2\ g^{-1}$). To increase this external area value, other strategies such as postsynthesis treatment with hydrogen peroxide under microwave irradiation has been reported,[34] creating mesopores within the ETS-10 structure that increased the external surface area of this material up to 70 $m^2\ g^{-1}$.

Table 1 Textural properties of the different samples

| ETS-10 sample | $S_{BET}$ ($m^2\ g^{-1}$) | $S_{ext}$ ($m^2\ g^{-1}$) | Particle size (μm) |
|---|---|---|---|
| Conventional $TiCl_3$_230_24 h | 289 ± 4 | 20 | 1.9 × 2.3[a] |
| Ti2_180_48 h | 206 ± 5 | 30 | 0.44 × 0.21[a] |
| $TiCl_3$_180_48 h | 94 ± 0 | 59 | 0.08 ± 0.02 |
| $TiCl_3$_180–230_48–2 h | 318 ± 5 | 42 | 1.2 ± 0.2 |
| $TiCl_3$_180–230_48–24 h | 166 ± 3 | 41 | 1.9 ± 0.3 |

[a] The first value corresponds to crystal size in direction $c$, and the second value to crystal size in directions $a = b$.[32]

## 3.2. Characterization of the membranes

**3.2.1. ETS-10 MMMs based on polysulfone (PSF).** Fig. 4 shows SEM images of the different ETS-10 MMMs based on PSF. The filler is distributed homogeneously within the polymer and an intimate filler–polymer interaction is suggested, especially for samples $TiCl_3$_180–230_48–2 h and $TiCl_3$_180–230_48–24 h (Fig. 4c and d) where, due to the roughness of the polycrystalline particles, polymer chains may enter into the intercrystalline spaces, giving rise to an interpenetrated filler–polymer composite.[31] Some particle agglomeration can be observed for samples Ti2_180_48 h and $TiCl_3$_180_48 h (Fig. 4a and b) due to the small particle size of these fillers.

Table 2 and Fig. 5 show the gas separation results for the $CO_2$/$CH_4$ mixture of 10 wt% MMMs based on PSF with different ETS-

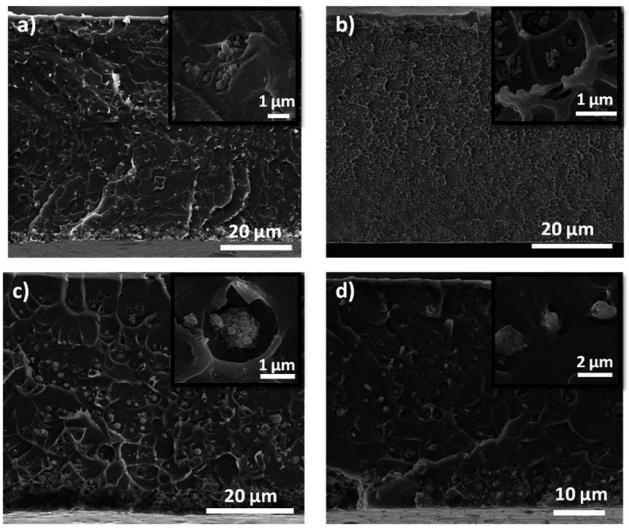


Fig. 4 SEM images of cross-sections of 10 wt% MMMs based on PSF with different ETS-10 samples, (a) Ti2_180_48 h, (b) $TiCl_3$_180_48 h, (c) $TiCl_3$_180–230_48–2 h, (d) $TiCl_3$_180–230_48–24 h.

10 samples. For Ti2_180_48 h and $TiCl_3$_180_48 h MMMs, the ETS-10 agglomerations observed by SEM created voids between the particles that could explain the decrease in $CO_2/CH_4$ selectivity. In addition, the slight decrease in $CO_2$ permeability could be due to the low porosity of $TiCl_3$_180_48 h sample and the presence of non-porous anatase as impurity in the Ti2_180_48 h sample. MMMs using samples $TiCl_3$_180–230_48–2 h and $TiCl_3$_180–230_48–24 h as fillers increased both their $CO_2$ permeability and $CO_2/CH_4$ selectivity in comparison with pure polymer. This can be explained by the fact that, in addition to the high porosity of these fillers and the good filler–polymer interaction, ETS-10 preferentially adsorbs $CO_2$ over $CH_4$,[35] probably because of the significantly greater quadrupole moment and polarizability of $CO_2$ molecules. Furthermore, adsorbed $CO_2$ is expected to reduce the $CH_4$ permeation by hindrance, resulting in overall $CO_2$ selectivity in $CO_2/CH_4$ mixtures.[17] Thus, because of two concomitant effects, *i.e.*, the diffusion and sorption paths created in the membrane when ETS-10 crystals are added and the optimized filler–polymer contact, the pursued trend of increasing both the permeability and selectivity with the addition of the filler was achieved.

Table 2 Gas separation results for ETS-10 MMMs at 10 wt% loading for equimolar $CO_2/CH_4$ mixtures at 35 °C, $\Delta P = 205$ kPa. Pure PSF values are the average and standard deviation of three different membranes

| Sample | $CO_2$ permeability (Barrer) | Selectivity $CO_2/CH_4$ |
|---|---|---|
| Pure PSF | 6.1 ± 0.2 | 31 ± 1 |
| Ti2_180_48 h | 5.4 | 28 |
| $TiCl_3$_180_48 h | 5.6 | 29 |
| $TiCl_3$_180–230_48–2 h | 7.8 | 38 |
| $TiCl_3$_180–230_48–24 h | 7.2 | 40 |

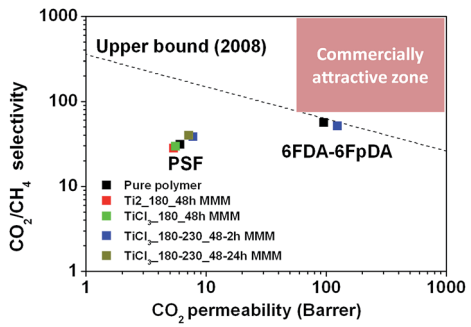


Fig. 5 Results of pure polymers and 10 wt% MMMs for $CO_2/CH_4$ mixture at 35 °C.

**3.2.2. 6FDA-6FpDA membranes.** In order to improve the performance of the MMMs, the more permeable polyimide 6FDA-6FpDA was chosen as the polymeric matrix. Table 3 shows the results obtained for the separation of $CO_2/CH_4$ mixtures using pure 6FDA-6FpDA membranes. For the separation of $CO_2/CH_4$ equimolar mixtures, $CO_2$ permeability of 96 ± 1 Barrer (in comparison with 6.1 ± 0.2 Barrer for pure PSF) with a $CO_2/CH_4$ selectivity of 56 ± 3 (31 ± 1 for pure PSF) were obtained. These high values can be explained because of the presence of bulky groups ($-CF_3$) that increase the free volume and make the structure stiffer, leading to more permeable and selective membranes. In addition, the high solubility of the condensable $CO_2$ gas in the polymer and its lower kinetic diameter (0.33 nm) in comparison with $CH_4$ (0.38 nm) also contribute to obtain simultaneously high permeability and selectivity for this mixture, being close to the 2008 Robeson upper bound.[36] It is worth mentioning that the single gas measurements were similar to those reported in the literature based on the "time lag" method, at 35 °C and 1 bar (see Table 3, errors corresponding to membranes manufactured with different solvents).[22] The fact that ideal selectivity (from single gas measurements) was lower than that obtained with binary mixtures suggests an apparent competitive adsorption of the gases favorable to $CO_2$. In consequence, in binary mixtures the permeability of $CH_4$ decreases due to the faster diffusion of the smaller and more strongly adsorbed $CO_2$ gas molecule.[29] Furthermore, $CO_2$ permeability was higher for the binary mixture than for single gas. Since the total feed pressure was kept constant, the $CO_2$ partial pressure gradient was double for single gas measurements than for those with a binary mixture.

Table 3 $CO_2/CH_4$ gas separation results for pure 6FDA-6FpDA membranes at 35 °C

| Measurement | $CO_2$ permeability (Barrer) | $CO_2/CH_4$ selectivity |
|---|---|---|
| Binary mixture ($\Delta P = 205$ kPa) | 96 ± 1[a] | 56 ± 3[a] |
| Single gas ($\Delta P = 205$ kPa) | 85.1 | 41.3 |
| Single gas "time lag" method (literature)[22] ($\Delta P = 101$ kPa) | 73 ± 6[b] | 44 ± 2[b] |

[a] The standard deviation was calculated from two different membranes. [b] The standard deviation was calculated from membranes prepared with different solvents (dichloromethane, tetrahydrofuran, *N*,*N*-dimethylacetamide, *N*,*N*-dimethylformamide and acetone).

Thus, as the $CO_2$ pressure increases, the membrane become saturated and therefore the permeability decreases.[37]

**3.2.3. ETS-10 MMMs based on 6FDA-6FpDA.** From the results obtained with ETS-10/PSF MMMs, $TiCl_3$_180–230_48–2 h was chosen for the preparation of MMMs based on 6FDA-6FpDA. This polycrystalline filler had the smallest particle size (1.2 μm) and the highest BET area and in consequence gave the best membrane performance in the PSF matrix (7.8 Barrer of $CO_2$ permeability together with $CO_2/CH_4$ selectivity of 38). Even though SEM images of ETS-10 MMMs at 10 wt% and 20 wt% loading (Fig. 6a and b, respectively) suggest an interpenetrated filler–polymer interaction, which could be a result of H-bonding between the external ETS-10 hydroxyl groups[38] and the imide groups of the polyimide, a decrease in selectivity with the addition of the filler indicates the presence of some defects, as will be discussed below. Particle agglomeration at 20 wt% filler loading can be observed, especially at the bottom of the membrane.

The XRD pattern of the MMMs (Fig. 7) matches the pattern of the filler, and the signal peaks related to ETS-10 increased with the filler loading, confirming that the particles preserved their structure inside the polymeric matrix.

Compared to bare polymer, ETS-10 MMMs based on 6FDA-6FpDA with 10 wt% loading showed an improvement in the $CO_2$ permeability from 96 ± 1 to 125 ± 1 Barrer, with a slight decrease in $CO_2/CH_4$ selectivity from 56 ± 3 to 51 ± 2 (Fig. 5). The fact that $CO_2/CH_4$ selectivity did not improve with the addition of ETS-10 could be explained from the selectivity value reported for ETS-10 for $CO_2/N_2$ mixtures (similar to $CO_2/CH_4$ mixtures) using a continuous ETS-10 membrane.[17] Although defects along the continuous ETS-10 membrane could modify this value, the reported $CO_2/N_2$ selectivity was 10.8, much lower than that for the 6FDA-6FpDA polymer. In the case of the MMMs, the defects may correspond to the ETS-10-6FDA-6FpDA polymer gaps or non-selective transport pathways through the intercrystalline spaces of the ETS-10 particles, since the ideal $CO_2/CH_4$ selectivity for ETS-10 crystals (calculated from adsorption data in the Henry's law region using the Langmuir equation) is 357 at 25 °C.[35] When higher amounts of this filler were added (20 wt%), the permeability increased to 183 Barrer but the $CO_2/CH_4$ selectivity dramatically decreased to 13, due to the increase in the formation of non-selective filler–polymer voids caused by particle agglomeration at high loadings. It can be said that the presence of defects in 6FDA-6FpDA based MMMs do not compensate, in terms of separation performance, the enhancement achieved in the filler–polymer interaction by modification of the textural properties of the filler. In any event, the $CO_2/CH_4$ separation performance of pure polymer and 10 wt% ETS-10 MMM are represented in the 2008 Robeson upper bound (Fig. 5), where the results obtained with these membranes are close to the commercially attractive zone.

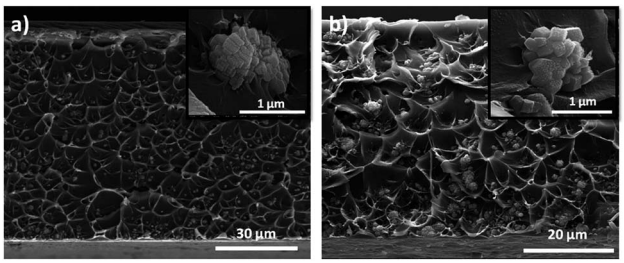


Fig. 6 SEM images of cross-sections of $TiCl_3$_180–230_48–2 h MMMs based on 6FDA-6FpDA with different filler loadings, (a) 10 wt%, (b) 20 wt%.

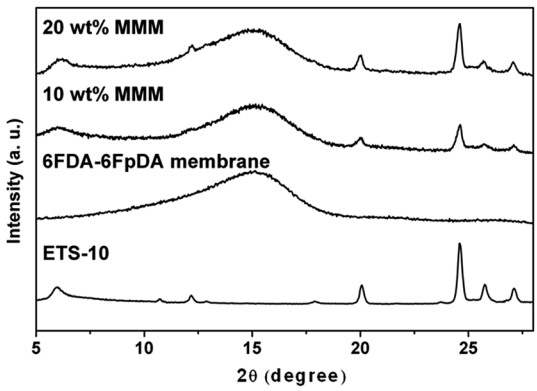


Fig. 7 XRD patterns of $TiCl_3$_230_24 h ETS-10, polyimide 6FDA-6FpDA and $TiCl_3$_180–230_48–2 h ETS-10 MMMs (10 and 20 wt% loading).

## 4. Conclusions

Adjusting the synthesis conditions (Ti source and synthesis time and temperature) enabled titanosilicate ETS-10 crystalline particles with different sizes and roughness to be obtained. The effect of these parameters on the separation performance was studied using polysulfone as the polymeric matrix. When ETS-10 syntheses were carried out in two steps ($TiCl_3$_180–230_48–2 h and $TiCl_3$_180–230_48–24 h samples), polycrystalline particles of 1–2 μm in size with high roughness and porosity were obtained, leading to a better filler dispersion and filler–polymer interaction with the polymer matrix. Their use as filler increased the permeoselectivity of pure polysulfone and improved the permeability of polyimide 6FDA-6FpDA membranes, giving results close to the Robeson upper bound. In addition, for polyimide 6FDA-6FpDA membranes the effect of working with individual gases rather than $CO_2/CH_4$ mixture on the membrane performance was also studied, suggesting a $CO_2$ preferential adsorption that enhanced the $CO_2/CH_4$ separation ability of the MMMs.

## Acknowledgements

Financial support from the Spanish Ministry of Economy and Competitiveness (MAT2011-25513, MAT2013-45071-R and MAT2013-40556-R) and DGA Program fellowships (S. S.) from the Regional Government of Aragón (T05) and the ESF are gratefully acknowledged. We acknowledge the use of the Servicio General de Apoyo a la Investigación-SAI (Universidad de Zaragoza). All the microscopy work was done in the Laboratorio de Microscopías Avanzadas at the Instituto de Nanociencia de Aragón (LMA-INA). The authors acknowledge the LMA-INA for offering access to their instruments and expertise.

## References

1 A. Anson, Y. Wang, C. C. H. Lin, T. M. Kuznicki and S. M. Kuznicki, *Chem. Eng. Sci.*, 2008, **63**, 4171–4175.
2 J. H. Choi, S. D. Kim, Y. J. Kwon and W. J. Kim, *Microporous Mesoporous Mater.*, 2006, **96**, 157–167.
3 S. M. Kuznicki, US Patent no. 4853202, 1989.
4 Z. Ji, B. Yilmaz, J. Warzywoda and A. Sacco Jr, *Microporous Mesoporous Mater.*, 2005, **81**, 1–10.
5 C. Casado, Z. Amghouz, J. R. García, K. Boulahya, J. M. González-Calbet, C. Téllez and J. Coronas, *Mater. Res. Bull.*, 2009, **44**, 1225–1231.
6 X. Wang and A. J. Jacobson, *Chem. Commun.*, 1999, 973–974.
7 M. Navarro, E. Mateo, B. Diosdado, M. Tsapatsis and J. Coronas, *RSC Adv.*, 2015, **5**, 18035–18040.
8 L. Tosheva and V. P. Valtchev, *Chem. Mater.*, 2005, **17**, 2494–2513.
9 S. B. Tantekin-Ersolmaz, C. Atalay-Oral, M. Tatlıer, A. Erdem-Senatalar, B. Schoeman and J. Sterte, *J. Membr. Sci.*, 2000, **175**, 285–288.
10 B. Seoane, J. M. Zamaro, C. Tellez and J. Coronas, *RSC Adv.*, 2011, **1**, 917–922.
11 T. S. Chung, L. Y. Jiang, Y. Li and S. Kulprathipanja, *Prog. Polym. Sci.*, 2007, **32**, 483–507.
12 M. Rezakazemi, A. Ebadi Amooghin, M. M. Montazer-Rahmati, A. F. Ismail and T. Matsuura, *Prog. Polym. Sci.*, 2014, **39**, 817–861.
13 M. M. Khan, V. Filiz, G. Bengtson, S. Shishatskiy, M. M. Rahman, J. Lillepaerg and V. Abetz, *J. Membr. Sci.*, 2013, **436**, 109–120.
14 A. Brunetti, F. Scura, G. Barbieri and E. Drioli, *J. Membr. Sci.*, 2010, **359**, 115–125.
15 I. Tiscornia, S. Irusta, P. Prádanos, C. Téllez, J. Coronas and J. Santamaría, *J. Phys. Chem. C*, 2007, **111**, 4702–4709.
16 I. Tiscornia, S. Irusta, C. Téllez, J. Coronas and J. Santamaría, *J. Membr. Sci.*, 2008, **311**, 326–335.
17 I. Tiscornia, I. Kumakiri, R. Bredesen, C. Téllez and J. Coronas, *Sep. Purif. Technol.*, 2010, **73**, 8–12.
18 F. X. L. i. Xamena and A. Zecchina, *Phys. Chem. Chem. Phys.*, 2002, **4**, 1978–1982.
19 P. Burmann, B. Zornoza, C. Téllez and J. Coronas, *Chem. Eng. Sci.*, 2014, **107**, 66–75.
20 C. Casado-Coterillo, F. Andrés, C. Téllez, J. Coronas and Á. Irabien, *Sep. Sci. Technol.*, 2014, **49**, 1903–1909.
21 D. F. Sanders, Z. P. Smith, R. Guo, L. M. Robeson, J. E. McGrath, D. R. Paul and B. D. Freeman, *Polymer*, 2013, **54**, 4729–4761.
22 R. Recio, L. Palacio, P. Prádanos, A. Hernández, Á. E. Lozano, Á. Marcos, J. G. de la Campa and J. de Abajo, *J. Membr. Sci.*, 2007, **293**, 22–28.
23 R. Wang, C. Cao and T.-S. Chung, *J. Membr. Sci.*, 2002, **198**, 259–271.
24 R. Recio, L. Palacio, P. Prádanos, A. Hernández, Á. E. Lozano, Á. Marcos, J. G. de la Campa and J. de Abajo, *Desalination*, 2006, **200**, 225–226.
25 A. Tena, L. Fernández, M. Sánchez, L. Palacio, A. E. Lozano, A. Hernández and P. Prádanos, *Chem. Eng. Sci.*, 2010, **65**, 2227–2235.
26 L. Lv, F. Su and X. S. Zhao, *Microporous Mesoporous Mater.*, 2004, **76**, 113–122.
27 D. M. Muñoz, J. G. de la Campa, J. de Abajo and A. E. Lozano, *Macromolecules*, 2007, **40**, 8225–8232.
28 D. M. Muñoz, M. Calle, J. G. de la Campa, J. de Abajo and A. E. Lozano, *Macromolecules*, 2009, **42**, 5892–5894.
29 S. Sorribas, B. Zornoza, C. Tellez and J. Coronas, *J. Membr. Sci.*, 2014, **452**, 184–192.
30 J. Rocha, A. Ferreira, Z. Lin and M. W. Anderson, *Microporous Mesoporous Mater.*, 1998, **23**, 253–263.
31 B. Zornoza, O. Esekhile, W. J. Koros, C. Tellez and J. Coronas, *Sep. Purif. Technol.*, 2011, **77**, 137–145.
32 N. C. Jeong, M. H. Lee and K. B. Yoon, *Angew. Chem., Int. Ed.*, 2007, **46**, 5868–5872.
33 N. C. Jeong, Y. J. Lee and K. B. Yoon, *Microporous Mesoporous Mater.*, 2008, **115**, 308–313.
34 C. C. Pavel, R. Palkovits, F. Schüth and W. Schmidt, *J. Catal.*, 2008, **254**, 84–90.
35 F. Mani, J. A. Sawada and S. M. Kuznicki, *Microporous Mesoporous Mater.*, 2015, **204**, 43–49.
36 L. M. Robeson, *J. Membr. Sci.*, 2008, **320**, 390–400.
37 C. A. Scholes, G. Q. Chen, G. W. Stevens and S. E. Kentish, *J. Membr. Sci.*, 2010, **346**, 208–214.
38 P. D. Southon and R. F. Howe, *Chem. Mater.*, 2002, **14**, 4209–4218.

 